RSC Advances

PAPER

View Article Online
View Journal | View Issue

On the stability of CdSe quantum dot-sensitized solar cells†

Cite this: *RSC Adv.*, 2014, **4**, 15702

Ke Wang, Weiwei He, Luo Wu, Guoping Xu, Shulin Ji and Changhui Ye*

Received 3rd March 2014
Accepted 17th March 2014

DOI: 10.1039/c4ra01846j

www.rsc.org/advances

The stability issues of CdSe quantum dot-sensitized solar cells have been investigated in this work. Stability is one of the most relevant issues for the real-world applications of quantum dot-sensitized solar cells. We find that CdSe quantum dots deposited in air are prone to oxidation, and when the solar cells are left in air for several months, CdSe quantum dots decompose partially to form Se particles and nanoribbons. The surface oxidation and the decomposition of CdSe quantum dots worsen all the parameters of the solar cells. Electrochemical impedance characterization provides unambiguous evidence for the evolution of the cells in the ageing process, which accounts for the observed performance worsening phenomena. Preparation under an inert atmosphere suppresses to some extent the degradation of the cells. These findings have significant implications for designing viable, high-performance quantum dot-sensitized solar cells.

1. Introduction

Quantum dot (QD)-sensitized solar cells (QDSCs) have attracted wide research attention in recent years. Quantum dots (QDs) can provide the possibility of harvesting hot electrons and generating multiple charge carriers with a single photon.[1–3] QDs are widely utilized as light absorbers in solar cells because of their tunability of optical properties depending on their size, their high extinction coefficient, and their built-in dipole moment facilitating the charge carrier separation.[4–10] So far, QDs of a wide range of materials have been investigated as photosensitizers, such as CdS,[11,12] CdTe,[13,14] PbS,[15,16] and PbSe.[17] Among the QDs materials, CdSe QDs offer new opportunities for harvesting light energy in the visible region of the solar spectrum.[18–20] Several methods have been employed to deposit CdSe QDs onto the photoanodes, for example, bifunctional linker molecule attachment[21] and successive ionic layer adsorption (SILAR)[22] methods are both highly successful in forming thickness-controlled layers of CdSe QDs. The SILAR process has been used to prepare various QD-sensitized photoelectrodes and offered an easy fabrication process as well as one of the most efficient QDSCs to date. CdSe QDs over nanoporous TiO_2 films were first fabricated by reducing the corresponding dioxide precursor in ethanol, which allows SILAR growth of CdSe QDs.

Recent efforts in improving the performance of CdSe QDSCs include the growth of CdS buffer layer,[23–25] the use of ZnS passivating layer,[26,27] the adoption of counter electrodes with higher activity (for example, CuS/CoS),[28,29] the incorporation of light scattering layer,[30] and the design of complex photoanode structures.[31,32] So far, CdSe QDSCs with the power conversion efficiency larger than 5% under simulated AM 1.5 have been demonstrated by several groups.[33–36] In our previous work, we have shown the positive effect of ZnS passivating layer on improving the photovoltaic properties of $CuInS_2$ QDSCs.[37] Recently, there have been some reports on how the thickness of the passivating layer affects the cell parameters,[23,38,39] such as the short-circuit current density (J_{sc}), the open-circuit voltage (V_{oc}), the fill factor (FF), and the overall efficiency (η). More importantly, it is well-known that CdSe QDs suffer from the stability issue in the air atmosphere, however, the stability study of CdSe QDSCs has rarely been reported in the literature.

In this work, we report on the effect of the thickness of ZnS passivating layer on the performance of CdSe QDSCs, the in-depth investigation of the stability of the cells aged in the air atmosphere, and the study of the mechanism for the performance degradation *via* electrochemical measurements. We propose future research direction to tackle the fast degradation issue of CdSe QDSCs.

2. Experimental

2.1 Methods

Preparation of the photoelectrode. The fluorine-doped SnO_2 (FTO) glass substrates were ultrasonically cleaned in ethanol, acetone, and deionized water for 30 min. An aqueous slurry of Degussa P25 TiO_2 nanoparticles were prepared by grinding 0.45 g of TiO_2 powder with 2 mL of ethanol, 200 μL of acetylacetone, and 200 μL of Triton X100. Then the nanoporous TiO_2

Key Laboratory of Materials Physics and Anhui Key Laboratory of Nanomaterials and Technology, Institute of Solid State Physics and Key Laboratory of New Thin Film Solar Cells, Chinese Academy of Sciences, Hefei 230031, China. E-mail: chye@issp.ac.cn; Fax: +86-551-65591434; Tel: +86-551-65595629

† Electronic supplementary information (ESI) available. See DOI: 10.1039/c4ra01846j

film was prepared by doctor-blading the slurry on the cleaned FTO and annealing at 450 °C for 30 min. *In situ* growth of CdSe QDs with the SILAR method was carried out by successive immersion of TiO_2 electrodes in ionic precursor solutions of Cd^{2+} and Se^{2-}. The concentration of Cd^{2+} ionic precursor solution is 0.1 M, which was prepared by dissolving 1.542 g $Cd(NO_3)_2$ in 50 mL ethanol. The concentration of Se^{2-} ionic precursor solution is 0.1 M, which was prepared by dissolving 0.378 g $NaBH_4$ and 0.555 g SeO_2 in 50 mL ethanol. The dipping time was 30 s for each. Following each immersion, the electrodes were rinsed in ethanol for 1 min in order to remove excessive precursor ions. Six cycles were applied to deposit CdSe QDs. After the deposition of CdSe QDs, 0.1 M $Zn(NO_3)_2$ in ethanol and 0.1 M Na_2S in methanol–water (7 : 3, v/v) were employed for the deposition of ZnS passivating layer up to 6 cycles. The photoelectrodes were alternately dipped into the two solutions for 1 min for each dipping followed by rinsing in ethanol for 1 min.

Preparation of CuS counter electrodes. A certain volume of 0.05 M $Cu(NO_3)_2$ in methanol was spin-coated on properly cleaned FTO substrate at 1600 rpm for 1 min and repeated twice. The coated FTO substrate was then immersed in Na_2S solution (0.05 M Na_2S in methanol–water(1 : 1, v/v)) for 1 min. Following each immersion, the obtained electrode was rinsed in methanol for 1 min and dried at 120 °C for 1 min. Six cycles were applied to prepare CuS counter electrodes.

Assembly of CdSe QDSCs. The assembly of a complete QDSC (active area: 0.06 cm^2) was carried out according to the following procedure. The CdSe/ZnS/TiO_2 photoelectrode and the counter electrode were sandwiched between a 20 μm-thick hot-melt ionomer film (Surlyn) under heating (145 °C, 20 s). Polysulfide electrolyte was composed of 1 M S and 1 M Na_2S in methanol–water (1 : 1, v/v). CdSe QDSCs without the passivation layer of ZnS was assembled similarly. Encapsulation of the cell was performed with a thin layer of polydimethylsiloxane (PDMS).

2.2 Characterization

FEI Sirion 200 field-emission scanning electron microscope (SEM) was used to study the morphology of the electrodes. The microstructure of CdSe QD-sensitized nanoporous TiO_2 films were investigated using transmission electron microscope (TEM, JEM 2010). Electrochemical impedance spectrum (EIS) and cyclic voltammetry (CV) were carried out on an electrochemical workstation (IM6ex, Zahner). The cells were illuminated using a solar simulator (Oriel 3A) at one sun (AM 1.5, 100 mW cm^{-2}). For the stability test, the cells were left in dark in environment atmospheres for a certain number of days.

3. Results and discussion

3.1 Structure of the photoanodes and the QDSC

The photoanode consists of nanoporous TiO_2 film with an average thickness ~15 μm as shown in the cross-sectional SEM image in Fig. 1(a). CdSe QDs were deposited by the SILAR method on the surface of nanoporous TiO_2 films, and the well-crystallized CdSe QDs can be observed clearly (Fig. 1(b)). The

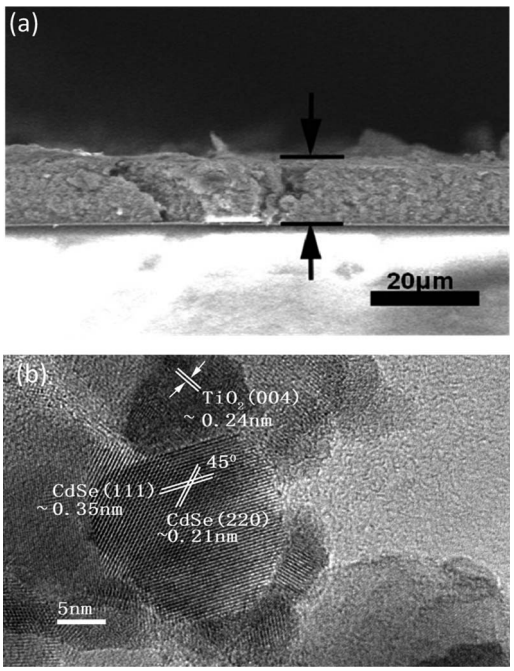

Fig. 1 SEM image of TiO_2 photoelectrode sensitized with CdSe QDs (a) and TEM image of CdSe QDs (b).

lattice fringes in the HRTEM image of the QDs correspond well to (111) and (220) lattice planes of CdSe. Similar to the observations in the literature, the size of CdSe QDs by the SILAR method is not homogeneous.

The structure of the CdSe QDSC is schematically illustrated in Fig. 2(a), where the light is illuminated from the photoanode

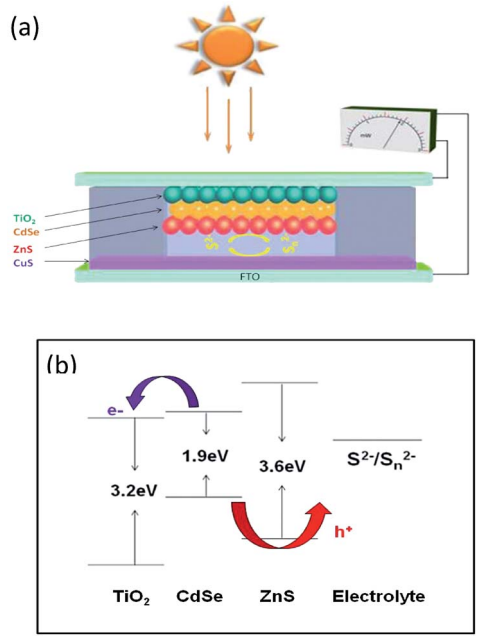

Fig. 2 Schematic illustration of the configuration of the CdSe QDSC (a) and energy level alignment of the electrode materials and the electrolyte (b).

side. The alignment of the energy levels of the electrode materials and the polysulfide electrolyte is exhibited in Fig. 2(b), where the photogenerated electrons flow to TiO_2 electrode and photogenerated holes flow to polysulfide redox couples.

3.2 Performance of CdSe QDSCs

We have measured the performance of CdSe QDSCs with 2 layers of ZnS passivation. As shown in Fig. 3, CdSe QDSCs with J_{sc} larger than 17 mA cm^{-2}, V_{oc} around 0.6 V, FF larger than 45%, and η larger than 5% have been fabricated with good reproducibility in our lab (Table 1).

The performance of CdSe QDSCs depends on many factors, such as the actual device area and the thickness of ZnS passivating layer (Fig. 3, 4, S1 and S2, Tables 1, 2and S1†).

It is well-known that ZnS passivating layer plays a critical role in suppressing the interfacial recombination and facilitating the transport of charge carriers.[1,23,24] The thickness of ZnS passivating layer may have an important consequence on the performance of the solar cells. We have studied the variation of the cell performance with the thickness of ZnS. We have also included a cell without ZnS passivation layer as a comparison. As shown in Fig. 4(a), the performance of CdSe QDSCs indeed varies dramatically with the thickness of ZnS passivating layer (also shown in Table 2 and Fig. S2†). All the four cell parameters decrease with the increase of the number of ZnS passivating layer when the layer thickness is larger than two. However, with one layer of ZnS, the surface passivation is not complete. These observations implies that the thickness of ZnS should be limited to a small value to allow efficient transport of charge carriers, and be thick enough to allow full passivation. The thickness of one layer of ZnS was found to be smaller than 10 nm.

In our experiment, two layers of ZnS work the best in improving the performance of CdSe QDSCs. We obtained approximate series and shunt resistance values by calculating the slopes at the open-circuit and the short-circuit voltages. The series resistance mainly stems out from the resistance of the photoelectrode, the electrolyte, the metal lead, and the contact between the electrodes and the metal lead. The variation of the series resistance was mainly contributed by the resistance change of the photoelectrode. The shunt resistance is the transfer resistance or recombination resistance at the solid–liquid junction between the photoelectrode and the redox couple. As the series resistance (R_s) of the solar cells increases with the increase of the thickness of ZnS when the thickness is larger than two layers (Fig. 4(b)), the decrease of J_{sc} is reasonable. Regarding the decrease of V_{oc}, it appears that the shunt resistance (R_{sh}) reduces to a much lower value for thicker ZnS (Fig. 4(b)), which implies that thicker ZnS layer may generate additional defect states either at the interface or in the bulk of ZnS layer and the leaking current worsens the V_{oc}. Therefore, the thickness of ZnS passivating layer should be kept thin enough to allow the efficient transport of charge carriers and sufficiently passivate the interfacial defect states.

Table 1 Performance of two CdSe QDSCs

	Sample 1	Sample 2
J_{sc} (mA cm^{-2})	17.73	17.90
V_{oc} (V)	0.60	0.60
FF (%)	47.84	46.60
η (%)	5.12	5.01

Comparing to the cell without ZnS passivation, the passivation mainly improves the photocurrent density, whereas it does not have pronounced effect on V_{oc} (Fig. 4(a)). This observation implies that ZnS passivation suppressed the charge trapping on surface states and generated more free charge carriers.

3.3 Stability of CdSe QDSCs

As we mentioned in the Introduction section, the stability issue for CdSe QDSCs is extremely important for the real-world applications. In this work, we mainly focus on two aspects of the stability issue. Firstly, we study how the preparation conditions (in air or in the glovebox) affect the performance of CdSe QDSCs, and then we investigate how the performance of CdSe QDSCs changes with ageing in air. In this part, two layers of ZnS were used and the only difference for the preparation conditions were either in air or in the glovebox, with all other experimental parameters being the same.

3.3.1 Effect of preparation conditions on the stability of CdSe QDSCs. As shown in Fig. 5(a), CdSe QDSC prepared in the glove box works much better than that prepared in air by the same preparation procedure (also shown in Table 3 and Fig. S3†). To our surprise, the series resistance of the cell

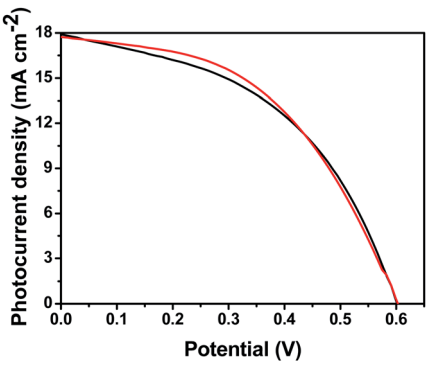

Fig. 3 J–V curves of two CdSe QDSCs.

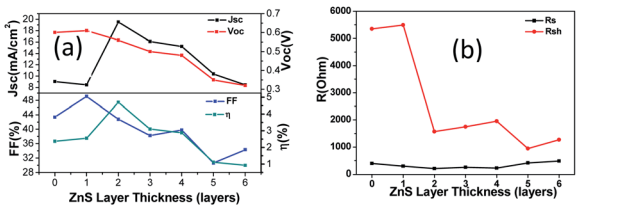

Fig. 4 Variation of the cell parameters J_{sc}, V_{oc}, FF, and η (a) and the resistance (b) with the thickness of ZnS passivating layer.

Table 2 J_{sc}, V_{oc}, FF, and η of CdSe QDSCs with the number of ZnS passivating layer

Number of layer	0 layer	1 layer	2 layers	3 layers	4 layers	5 layers	6layers
J_{sc} (mA cm^{-2})	9.03	8.45	19.53	16.10	15.24	10.38	8.42
V_{oc} (V)	0.60	0.61	0.56	0.50	0.48	0.35	0.32
FF (%)	43.36	49.08	42.76	38.25	39.81	30.61	34.31
η (%)	2.37	2.55	4.70	3.10	2.88	1.11	0.92

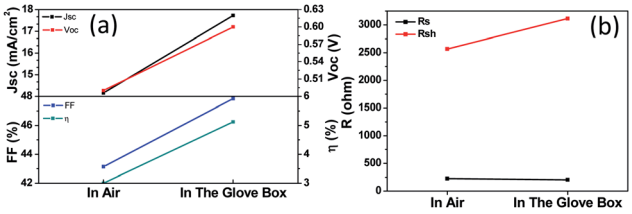

Fig. 5 Variation of the cell parameters J_{sc}, V_{oc}, FF, and η (a) and the resistance (b) of CdSe QDSCs prepared in air or in the glove box.

prepared in air is only slightly larger than that of the cell prepared in the glove box, which could partially account for the performance degradation of CdSe QDSCs. The decrease of J_{sc} could also be induced by the weaker visible light harvesting of CdSe QDs after oxidation. As shown in Fig. S4,† the cells prepared in air indeed exhibited dramatic decrease of the visible light absorption. The shunt resistance of the cell prepared in air is much smaller than that of the cell prepared in the glovebox, which indicates that the oxidation of CdSe QDs generates additional interfacial defects between CdSe QDs and TiO_2/ZnS, and these interfacial defects worsen FF and V_{oc}.

3.3.2 Effect of ageing on the stability of CdSe QDSCs. Performance degradation of QDSCs is a notorious problem. In this work, we find that the degradation of non-encapsulated CdSe QDSCs is rather fast and when the cell was left in room atmosphere for only one day, the efficiency loss of 40% was observed, and an efficiency loss more than 80% was observed for three-day's ageing (Fig. 6(a), Table 4, and Fig. S5†). The series and the shunt resistance both increases with the ageing process. Considering the results for the cells prepared in air, the ageing may cause the further oxidation of CdSe QDs. When the oxidation process continues, the series resistance will increase to some extent. Regarding the shunt resistance, the initial oxidation generates interfacial defects that decrease the shunt resistance as observed for the cell prepared in air (Fig. 5(b)), when more oxygen atoms incorporated, the interfacial defect density would decrease and the shunt resistance would increase to some extent (Fig. 6(b)). In the following section, we will see that the decomposition of CdSe QDs after long-term ageing to generate Se nanostructures contributes additionally to the decrease of the shunt resistance.

It was observed that although ZnS passivation could not completely prevent the degradation of the cells, we indeed found that the degradation rate was slowed down as compared with the cells without ZnS passivation (Fig. S6†).

We then examined the stability against ageing for encapsulated CdSe QDSCs (with 2 layers of ZnS passivation), and found that the degradation, although was much slower, was still took place (Fig. 7 and S7†). Therefore, the decomposition of CdSe must be seriously considered.

Table 3 J_{sc}, V_{oc}, FF, and η of CdSe QDSCs prepared in air or in the glove box

	In air	In the glove box
J_{sc} (mA cm^{-2})	14.15	19.53
V_{oc} (V)	0.49	0.56
FF (%)	43.14	42.76
η (%)	3.00	4.70

3.4 Electrochemical characterization of CdSe QDSCs

As shown in the previous section, after ageing in the air for different days, the cell decreased in performance. In order to gain in-depth understanding of the physical mechanism involved in the variation of the performance, we have measured the electrochemical impedance spectra of the cells aged for different days. From Fig. 8(a), we can see that when the reverse bias voltage increases from zero to 0.5 V, the arc of the impedance curve gets smaller, and when the bias voltage is larger than 0.5 V, the arc gets larger again (summarized in Fig. 8(b)). Therefore, for the cell aged for 1 day, the flat band voltage under dark should be close to 0.5 V, without considering the overpotential. We have compared cells aged for different days, and shown the impedance spectra under zero bias in Fig. 8(c). The arc of the impedance curves gets smaller for cells aged for more days, which indicates the decrease of the transfer resistance, similar to the concept of the shunt resistance in the previous sections. This observation further supports the generation of more interfacial defects with ageing. From the inset in Fig. 8(c), the series resistance gets larger for cells aged for more days (summarized in Table 5), which is also

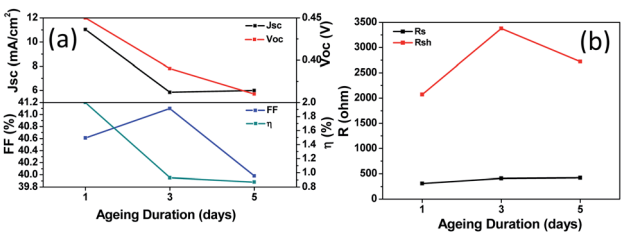

Fig. 6 Variation of the cell parameters J_{sc}, V_{oc}, FF, and η (a) and the resistance (b) of CdSe QDSCs aged for different days in air.

Table 4 J_{sc}, V_{oc}, FF, and η of CdSe QDSCs aged for different days

Time per day	1 day	3 days	5 days
J_{sc} (mA cm^{-2})	11.03	5.84	5.99
V_{oc} (V)	0.45	0.39	0.36
FF (%)	40.61	41.10	39.98
η (%)	2.00	0.93	0.87

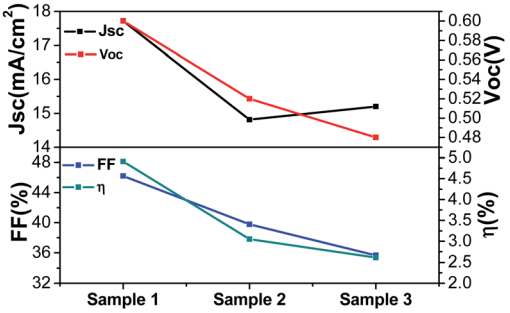

Fig. 7 Variation of the cell parameters J_{sc}, V_{oc}, FF, and η of encapsulated CdSe QDSCs aged for different days in air.

consistent to the trend shown in the previous section. However, it should be born in mind that the resistance values obtained in previous sections were measured by static I–V measurement, whereas in this section, the values were measured by stimulated techniques with a small AC input. Both these two techniques provide independent evidence of the increase of the series resistance and decrease of the shunt resistance of the cells under ageing process.

We have also measured the phase angle under different frequencies. As shown in Fig. 8(d), with the increase of the bias voltage, the peak of the phase angle curve shifts to higher frequency. This observation could be understood as follows. At the reverse bias regime, the capacitance corresponds approximately to the electrical double layer capacitance and varies slowly with the bias voltage. As the resistance decreases with the bias voltage, therefore, the RC constant decreases with the increase of the bias voltage, and consequently, the peak phase angle moves to higher frequency with the increase of the bias voltage. In addition, we can see from Fig. 8(e) that under zero bias voltage, the cell aged for 1 day exhibits only one peak in the phase angle curve, whereas for cells aged for 3 and 5 days, another peak appeared in higher frequency regime, and this new peak shifted to even higher frequency with the ageing process. Generally, response in high frequency indicates a bulk-like behavior. From the ageing experiments in the previous section, we can come to the conclusion that the oxidation of CdSe QDs generates more bulk-like defects in the QDs, which further decreases the performance of CdSe QDSCs.

As learned from the previous section that ageing causes the increase of the series resistance which is responsible for the reduction of J_{sc} and the decrease of the shunt resistance which causes the reduction of V_{oc}. To gain more insights into the reduction of V_{oc} with ageing in air, we have measured Mott–

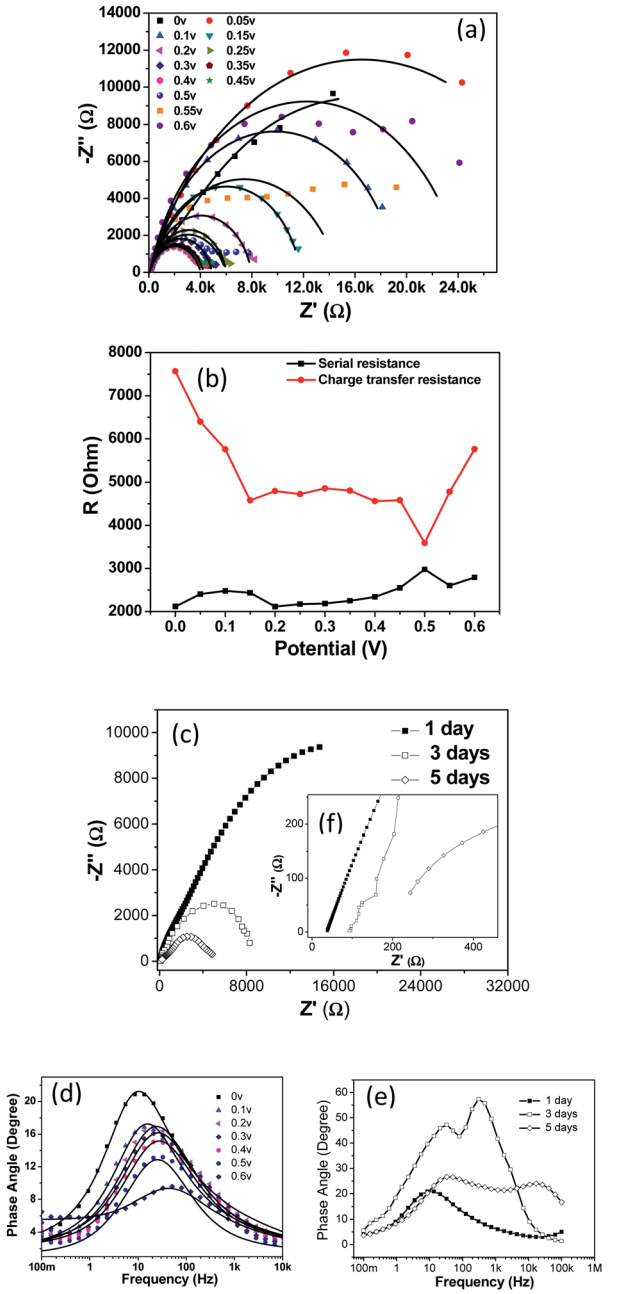

Fig. 8 Electrochemical impedance spectra of CdSe QDSCs aged for different days in air. Impedance spectrum under different bias voltage of the cell aged for 1 day (a), the series and charge transfer resistances of CdSe QDSCs under different bias voltage aged for 1 day (b), impedance spectrum under zero bias voltage of cells aged for different days (c), phase angle of the cell under different bias voltages (d), and phase angle under zero bias voltage of cells aged for different days (e). Inset in (c) is an enlarged portion at high frequency range of the curves.

Schottky (MS) curves for cells aged for different days. From Fig. 9, the extrapolated intercept in the potential coordinate axis in the two-electrode system corresponds approximately to the Schottky barrier height, and is also close to V_{oc}. As summarized in Table 5, with the ageing process, the Schottky barrier height decreases dramatically, and V_{oc} also decreases as observed in the previous sections.

As a comparison, the cells without ZnS passivation exhibited a higher series resistance (Fig. S8†), agreeing well to observations in the previous section. In a sharp contrast, the encapsulated cells showed a smaller series resistance which only gently increased from 39 to 43 Ω after an ageing period of 5 days (Fig. S9†). This observation further indicates that the performance degradation of the encapsulated cells might come from the degradation of CdSe QDs.

It is important to check the morphology change of CdSe QDs with ageing. Because the cells aged for several days do not exhibit vivid variation of morphology change, we instead examined a cell aged for 5 months. This cell shows poor performance (smaller than 1% overall efficiency). It is rather surprising that CdSe QDs show a drastic morphology change. As shown in Fig. 10(a), some long nanoribbons have been observed together with nanoparticles. Selected-area electron diffraction (SAED) pattern in the inset in Fig. 10(a) shows an ordered arrays of diffraction spots for the nanoribbon, indicating the good crystallinity of the nanoribbon. Energy dispersive spectroscopy (EDS) proves that the nanoribbons are elemental Se, instead of CdSe or SeO_2 (Fig. 10(b)). It is well-known that CdSe QDs are unstable in air because of the photo-oxidation in the presence of water or oxygen. Solar cells that involve CdSe QDs also suffer from the stability issues. In this case, even the cells stored under dark still exhibited the oxidation. Of course, we believe that the cell under the illumination of the solar simulator may accelerate the oxidation of CdSe QDs.

Saunders *et al.* discussed the phase separation of nanoparticle–polymer photovoltaic cells,[40] and Yang *et al.* reported

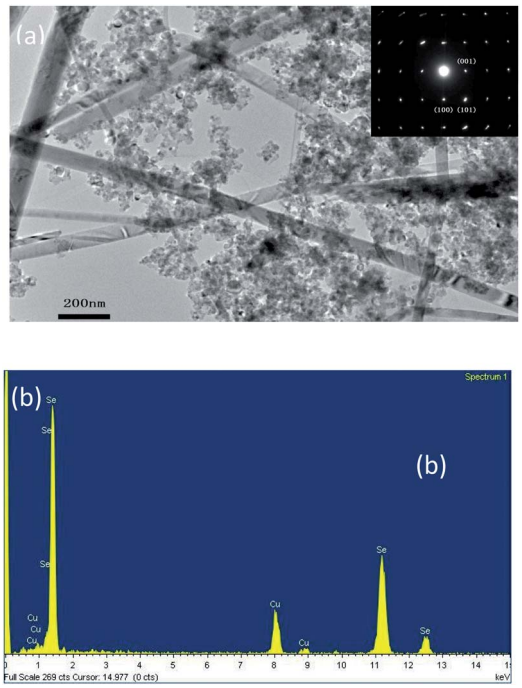

Fig. 10 TEM image (a) and EDS spectrum (b) of CdSe QDSCs aged for five months in air. Inset in (a) is the SAED pattern.

Table 5 Series resistance and Schottky barrier height of CdSe QDSCs aged for different days in air

	1 day	3 days	5 days
R_s (Ω)	38	92	244
V_{SB} (V)	0.71	0.40	0.18

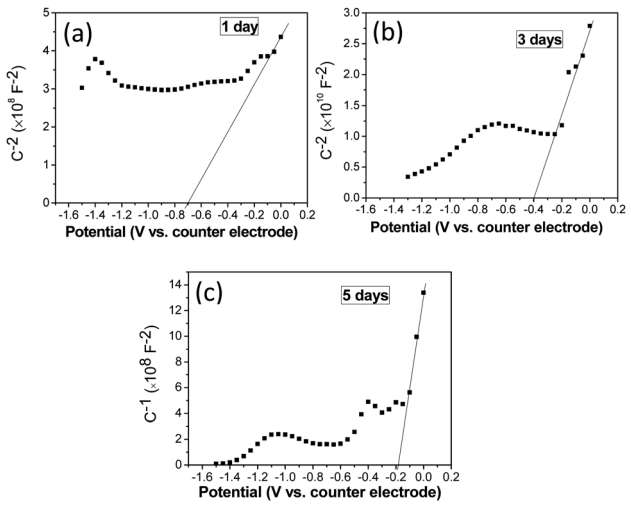

Fig. 9 MS plot of CdSe QDSCs aged for 1 day (a), 3 days (b), and 5 days (c) in air.

that hybrid polymer-CdSe solar cells degraded after being left in the air environment for merely a few hours.[41] In most cases, CdSe QDs could be oxidized at the surface. However, Se is an element with high equilibrium vapor pressure or high solubility in alkaline solution, and CdSe QDs tend to lose Se in long term ageing process. It is noted that there have been some reports on the growth of Se nanowires and nanoribbons *via* either vapor phase or solution phase processes.[42,43] Because of the inherent chain-like structure of Se molecules, Se tends to form quasi-one-dimensional structures such as nanowires and nanoribbons. It is not surprising that the oxidation of CdSe QDs causes the poor stability of the non-encapsulated cells, however, the formation of Se nanoribbons with ageing is interesting. Therefore, the phase separation of CdSe QDs entails further research work.

It is noteworthy that Se is a semiconductor, and the nanoribbons may cause severe shunting path in the cells and the performance of the cells would be degraded with time. This might be an additional reason for the observed decrease of the shunt resistance. Together with the increase of the series resistance induced by the oxidation of the QDs, the stability issue of CdSe QDSCs now is understood, and strategies should be devised to suppress both the oxidation and the phase separation of CdSe QDs in the working cells.

4. Conclusions

In summary, we have reported the fabrication of CdSe QDSCs with efficiency higher than 5%. We have throughly investigated the stability issue of CdSe QDSCs, and have found out that the surface oxidation and the phase separation of CdSe QDs dramatically worsened the performance of the cell. Further

development of the solar cells on the basis of CdSe QDs may entail the fabrication of all solid-state solar cells that do not involve liquid electrolyte, and a proper encapsulation of the cell is indispensable to make this device viable.

Acknowledgements

This work was supported by National Basic Research Program of China (973 Program, grant no. 2011CB302103), National Natural Science Foundation of China (grant no. 11274308), and the Hundred Talent Program of the Chinese Academy of Sciences.

Notes and references

1 R. D. Schaller and V. I. Klimove, *Phys. Rev. Lett.*, 2004, **92**, 186601.
2 O. E. Semonin, J. M. Luther, S. Choi, H.-Y. Chen, J. B. Gao, A. J. Nozik and M. C. Beard, *Science*, 2011, **334**, 1530–1533.
3 H. M. Zhu, Y. Yang and T. Q. Lian, *Nano Lett.*, 2013, **46**, 1270–1279.
4 I. Mora-Seró, S. Giménez, F. Fabregat-Santiago, R. Gómez, Q. Shen, T. Toyoda and J. Bisquert, *Acc. Chem. Res.*, 2009, **42**, 1848.
5 I. Mora-Seró and J. Bisquert, *J. Phys. Chem. Lett.*, 2010, **1**, 3046.
6 C. A. Leatherdale, W. K. Woo, F. V. Mikulec and M. Bawendi, *J. Phys. Chem. B*, 2002, **106**, 7619.
7 A. Kongkanand, K. Tvrdy, K. Takechi, M. Kuno and P. V. Kamat, *J. Am. Chem. Soc.*, 2008, **130**, 4007.
8 C. Chen, Y. Xie, G. Ali, S. H. Yoo and S. O. Cho, *Nanotechnology*, 2011, **22**, 015202.
9 A. J. Nozik, *Physica E*, 2002, **14**, 115.
10 M. Shim and P. Guyot-Sionnest, *J. Chem. Phys.*, 1999, **111**, 6955.
11 W. T. Sun, Y. Yu, H. Y. Pan, X. F. Gao, Q. Chen and L. M. Peng, *J. Am. Chem. Soc.*, 2008, **130**, 1124.
12 H. Choi, R. Nicolaescu, S. Paek, J. Ko and P. V. Kamat, *ACS Nano*, 2011, **5**, 9238.
13 X. F. Gao, H. B. Li, W. T. Sun, Q. Chen, F. Q. Tang and L. M. Peng, *J. Phys. Chem. C*, 2009, **113**, 7531.
14 G. Y. Lan, Z. Yang, Y. W. Lin, Z. H. Lin, H. Y. Liao and H. T. Chang, *J. Mater. Chem.*, 2009, **19**, 2349.
15 S. A. McDonald, G. Konstantatos, S. Zhang, P. W. Cyr, E. J. D. Klem, L. Levina and E. H. Sargent, *Nat. Mater.*, 2005, **4**, 138.
16 R. Plass, S. Pelet, J. Krueger and M. Grätzel, *J. Phys. Chem. B*, 2002, **106**, 7578.
17 R. J. Ellingson, M. C. Beard, J. C. Johnson, P. Yu, O. I. Micic, A. J. Nozik, A. Shabaev and A. L. Efros, *Nano Lett.*, 2005, **5**, 865.
18 R. Loef, A. J. Houtepen, E. Talgorn, J. Schoonman and A. Goossens, *Nano Lett.*, 2009, **9**, 856.
19 J. J. Li, Y. A. Wang, W. Guo, J. C. Keay, T. D. Mishima, M. B. Johnson and X. Peng, *J. Am. Chem. Soc.*, 2003, **125**, 12567.
20 H. Jin, S. Choi, R. Velu, S. Kim and H. J. Lee, *Langmuir*, 2012, **28**, 5417.
21 I. Robel, V. Subramanian, M. Kuno and P. V. Kamat, *J. Am. Chem. Soc.*, 2006, **128**, 2385.
22 H. Lee, M. Wang, P. Chen, D. R.Gamelin, S. M. Zakeeruddin, M. Grätzel and M. K. Nazeeruddin, *Nano Lett.*, 2009, **9**, 4221.
23 Z. X. Pan, H. Zhang, K. Cheng, Y. M. Hou, J. L. Hua and X. H. Zhong, *ACS Nano*, 2012, **6**, 3982.
24 Y. L. Lee and Y. S. Lo, *Adv. Funct. Mater.*, 2009, **19**, 604.
25 Y. L. Lee, C. F. Chi and S. Y. Liau, *Chem. Mater.*, 2009, **22**, 922.
26 Q. Shen, J. Kobayashi, L. J. Diguna and T. Toyoda, *J. Appl. Phys.*, 2008, **103**, 084304.
27 N. Guijarro, J. M. Campiña, Q. Shen, T. Toyoda, T. Lana-Villarreal and R. Gómez, *Phys. Chem. Chem. Phys.*, 2011, **13**, 12024.
28 Z. Yang, C. Y. Chen, C. W. Liu and H. T. Chang, *Chem. Commun.*, 2010, **46**, 5485.
29 Z. Yang, C. Y. Chen, C. W. Liu, C. L. Li and H. T. Chang, *Adv. Energy Mater.*, 2011, **1**, 259.
30 Q. Zhang, X. Guo, X. Huang, S. Huang, D. Li, Y. Luo, Q. Shen, T. Toyoda and Q. Meng, *Phys. Chem. Chem. Phys.*, 2011, **13**, 4659.
31 Z. L. Zhu, J. H. Qiu, K. Y. Yan and S. H. Yang, *ACS Appl. Mater. Interfaces*, 2013, **5**, 4000.
32 J. S. Luo, S. K. Karuturi, L. J. Liu, L. T. Su, A. Y. Tok and H. J. Fan, *Sci. Rep.*, 2012, **2**, 451.
33 M. A. Hossain, J. R. Jennings, C. Shen, J. H. Pan, Z. Y. Koh, N. Mathews and Q. Wang, *J. Mater. Chem.*, 2012, **22**, 16235.
34 H. Zhang, K. Cheng, Y. M. Hou, Z. Fang, Z. X. Pan, W. J. Wu, J. L. Hua and X. H. Zhong, *Chem. Commun.*, 2012, **48**, 11235.
35 Z. X. Pan, H. Zhang, K. Cheng, Y. M. Hou, J. L. Hua and X. H. Zhong, *ACS Nano*, 2012, **6**, 3982.
36 P. K. Santra and P. V. Kamat, *J. Am. Chem. Soc.*, 2012, **134**, 2508.
37 G. P. Xu, S. L. Ji, C. H. Miao, G. D. Liu and C. H. Ye, *J. Mater. Chem.*, 2012, **22**, 4890.
38 L. J. Diguna, Q. Shen, J. Kobayashi and T. Toyoda, *Appl. Phys. Lett.*, 2007, **91**, 023116.
39 H. M. Zhu, N. H. Song and T. Q. Lian, *J. Am. Chem. Soc.*, 2010, **132**, 15038.
40 B. R. Saunders and M. L. Turner, *Adv. Colloid Interface Sci.*, 2008, **138**, 1.
41 L. Qian, J. H. Yang, R. J. Zhou, A. W. Tang, Y. Zheng, T. K. Tseng, D. Bera, J. G. Xue and P. H. Holloway, *J. Mater. Chem.*, 2011, **21**, 3814.
42 B. Gates, B. Mayers, B. Cattle and Y. Xia, *Adv. Funct. Mater.*, 2002, **12**, 219.
43 X. Cao, Y. Xie and L. Li, *Adv. Mater.*, 2003, **15**, 1914.

